LBL-9244

# IN SEARCH OF HIGH DENSITY COLLECTIVE PHENOMENA IN NUCLEAR COLLISION

M. Gyulassy

Nuclear Science Division
Lawrence Berkeley Laboratory
Berkeley, California 94720

June 1979

ABSTRACT

The progress made toward uncovering signatures of collective phenomena is reviewed. Elements of the basic reaction mechanism leading to a complex background are first discussed. Possible hints of collective phenomena in proton and pion single and double inclusive spectra as well as $\pi^-$ multiplicity data are then described.

## I. INTRODUCTION

In the past year much progress has been made in the search for high density collective phenomena via relativistic nuclear collisions (0.2-2.0 GeV/nucleon). In this talk, I will review that progress and indicate the future directions along which this search will continue.

Before discussing collective phenomena though, it is important to review the basic reaction mechanism in nuclear collisions. That underlying reaction mechanism has been found to lead to a complex, non-trivial background that tends to obscure the signatures of collective phenomena. The primary accomplishments of the first generation of experiments and theoretical studies have been in fact the classification and clarification of the elements of that basic reaction mechanism.[1] Based on that knowledge, the second generation of more detailed experiment are now beginning to provide us with tantalizing hints of collective phenomena.

## II. ELEMENTS OF THE BASIC REACTION MECHANISM

### 1) Geometry and Impact Parameter

Perhaps the most crucial factors determining the reaction mechanism are the impact parameter $\tilde{b}$ and the geometry of the projectile $A_P$ and target $A_T$. The impact parameter determines the number of participant and spectator nucleons in the collision based on Glauber theory notions as employed in the Fireball, Firestreak, and Row on Row models.[1] The vector direction of $\tilde{b}$ defines the scattering plane and hence the relative orientation of participants

NOTICE
This report was prepared as an account of work sponsored by the United States Government. Neither the United States nor the United States Department of Energy, nor any of their employees, nor any of their contractors, subcontractors, or their employees, makes any warranty, express or implied, or assumes any legal liability or responsibility for the accuracy, completeness or usefulness of any information, apparatus, product or process disclosed, or represents that its use would not infringe privately owned rights.

and spectators. The number of participants controls the total energy and momentum transfer and thus the number of produced pions and the inelasticity of the collision. The orientation of spectator and participant matter determines certain final state interactions such as nuclear shadowing.

Geometry governs the magnitude of all reaction cross sections. Futhermore, there is a qualitative difference between symmetric $A_p=A_T$ and asymmetric $A_p<<A_T$ projectile target combinations. Some type of phenomena such as hydrodynamic side splash are best studied via $A_p<<A_T$ geometries. Other phenomena such as pion coherence are best studied via $A_p=A_T$ for which the yields are symmetrically distributed about the center of mass rapidity.

To avoid averaging over a large number of reaction types and mechanisms it is vital to select as narrow a range of $\tilde{b}$ as possible. Fortunately, we now have several handles[1] on controlling the range of impact parameters: 1) associated charged fragment multiplicities $P(M_{ch})$, 2) azymuthal distribution of associated multiplicities $P_m(\emptyset)$, 3) $\pi^-$ multiplicities and distributions $P(n_{\pi^-})$, and 4) Hanbury Brown and Twiss effect via $\pi^-\pi^-$ or pp correlations.

The mark of the second generation of experiments to be discussed below is the use of the above handles to control and specify the geometry of a class of events under study. In the future, increasingly sophisticated $4\pi$ trigger systems will be available to further restrict the geometry in nuclear collisions.

2) Momentum-Space Regions

Once a class of events with a well defined geometry is selected then the reaction mechanism appropriate to a particular region of phase space can be discussed. It has proven useful to plot momentum distributions in terms of a rapidity contour plot $(y, P_\perp)$ where $y = \tanh^{-1}(V_\parallel/c)$ is the relativistic longitudinal velocity and $P_\perp$ in the perpendicular momentum of the fragment.

In terms of the $(y, P_\perp)$ plane, we can readily distinguish between (1) the projectile fragmentation region centered at $(y_p,0)$, (2) the target fragmentation region centered at (0,0) and (3) the mid rapidity region centered near $(y_{cm},0)$. The reaction mechanism in the fragmentation regions involves mainly the spectator nucleons with small excitation energies in the projectile or target frames. The mid rapidity region involves the participant nucleons that have undergone multiple collisions. It is in this mid rapidity region where signatures of collective phenomena are likely to appear.

3) Multicomponent Nature of Spectra

Even after the geometry and the momentum space region are specified (eg. $b<< R_T$, $Y=y_p/2$) the yield is determined by the competition of several components. These components refer to the number of binary collisions, N, each nucleon has suffered in the interaction region.

Based on studies with the Row on Row model[1], Hufner, Knoll, and Randrup have found that there are basically three distinct components: 1) direct (N=1), 2) intermediate (N=2,3), 3) thermal (N >4). The direct or knock out component results from elementary nucleon-nucleon collisions averaged over the Fermi motion in nuclei. Calculations[1] of this component have been carried out by Hatch and Koonin. The intermediate component represents the non-equilibrated nucleons which have scattered only 2 or 3 times. Finally, there is the thermal or hydrodynamic component resulting from very many binary collisions, N> 4.

The relative weight of each component depends on $\tilde{b}$, $A_p$, $A_T$, and $E_p$. An extremely instructive example was calculated by Knoll and Randrup shown in Fig. 1. They first calculated the average number of mean free paths a projectile nucleon traverses at a distance $\tilde{s}$ from the center of the target A,

$$N_A(\tilde{s}) = \int dz\, \rho_A(z,\tilde{s})\, \sigma_{NN} \qquad (1)$$

using diffuse nuclear densities. Then the probability that a projectile nucleon suffered N collisions in traversing the target is given by

$$P_A(N) = \frac{\sigma_A(N)}{\sigma_A{}^{tot}} = \int \frac{d^2s}{\sigma_A{}^{tot}} \frac{(N_A(\tilde{s}))^N}{N!} e^{-N_A(\tilde{s})} \quad . \qquad (2)$$

In eq. (2), $\sigma_A{}^{tot} = \Sigma\sigma_A(N)$, N = 1, $\cdots$. In a central (b = 0) $A_p=A_T=A$ collision, the distribution of the number of projectile nucleons scattering N times is then proportional to $N\sigma_A(N)$ as in Fig. 1 b. Using the distribution in Fig. 1 b, we can construct a table showing the fraction of yield in each of the three components. See Table I. Note that these estimates include nuclear diffuseness and fluctuations. However, multiple collisions between two projectile or two target nucleons are not included. Neither are collisions between nucleons in adjacent tubes considered. We can nevertheless conclude from Table I that for collisions involving nuclei lighter than Ar + Ar, there is a major fraction of non-thermal component ∿50% of the total yield even at b=0!

Figure 1 and Table I also suggest that there may be qualitiative difference between Ar+Ar and U+U collisions. In the later, which will be experimentally feasible in a few years, the non equilibrium component is significantly smaller than in Ar+Ar. Since the collective phenomena are likely to be rather sensitive to the fraction of non-equilibrium component, this shows that we should not be too impatient in the search for collective phenomena at this point when Ar is the heaviest available projectile.

Table I also helps us understand why so many diverse models such as Firestreak, Hydrodynamic, and Cascade[1] all seem to reproduce the gross features of the spectra to within factors of 2-4. The thermal component in the absence of compression effects is determined by three general factors: (1) geometry, responsible for the magnitude, (2) Central limit theorem of

statistics leading to Gaussian spectra, (3) Energy-momentum conservation giving the mean and width of the Gaussian distributions. Since all models include this component to various degrees (50-100%) and since this component is determined by the general factors above, we may expect that to the level of a factor of 2-4 all models lead to similar gross features. However, the detailed feature of spectra will depend on the non-equilibrium component and possible compression effects that do differ from model to model. What these observations tell us is that we must look for more detailed comparisons with data if models are to be distinguished and collective effects are to be uncovered.

4) Final State Interactions

In the search for collective phenomena, also another important ingredient of the reaction mechanism must always be taken into account. That is the role of final state interaction. We now have clear evidence from Nagamiya et. al.[3] that nuclear shadowing occurs in C+Pb. This is one example of final state interactions between participant and spectator nucleons that leads to modifications of correlation data. The existence of strong Coulomb final state interaction has also been demonstrated by Benenson et. al.[4] in single $\pi^{\pm}$ inclusive cross sections.

A third type of final state interactions is composite fragment formation. Experimentally, up to 50% of all nucleons emerging from nuclear collisions end up in light composites d, $\alpha$, etc. Some of these composites may have been dynamically produced as in the chemical equilibrium models[5], but the coalescence model[6] seems to account for the observed composite spectra. The relation between the inclusive rate $d^3\sigma(A)/dk^3$, at a given momentum per nucleon, k, for fragment A and the proton inclusive rate $d^3\sigma(p)/dk^3$ is

$$\frac{d^3\sigma(A)}{dk^3} \propto \left(\frac{d^3\sigma(p)}{dk^3}\right)^A \qquad (3)$$

While the coalescence model motivates this result, theoretically the derivation of eq. (3) is still not well understood. Nevertheless, eq. (3) is found to be empirically satisfied.

The importance of composite formation is that any model of nuclear collisions treating only nucleon and pion degrees of freedom must be corrected by a large factor to take this form of final state interactions into account. This includes all models at present except the firestreak model, which, however, suffers itself from the neglect of the significant non-thermal component discussed above.

In practice, calculations without composite formation can be compared only to the primary charged inclusive spectra

$$d\sigma_{prim} = d\sigma\ (p) + d\sigma\ (d) + d\sigma\ (t) + 2\ d\sigma\ (\alpha) + \cdots \quad . \qquad (4)$$

Experimentally, $d\sigma_{prim}$ and $d\sigma(p)$ have different shapes and can differ in certain regions of phase space by factors of 2 or more. Only in low density regions of phase space such as mid rapidity, high $p_\perp$ is $d\sigma_{prim} \approx d\sigma\ (p)$.

In summary nuclear shadowing, Coulomb distortions, and composite formation contribute to the complex background on which signatures of collective phenomena must be sought.

## III. SIGNATURES OF COLLECTIVE PHENEOMENA

We now turn to the various observables used in the search. Table II summarizes those observables and the signatures sought and also indicates the experimental status of each. Before discussing these observables in turn, we should note a qualitative distinction between collective and coherent phenomena[7]. Collective refers to many body dynamical phenomena that can be characterized by a small set of variables such as shape or density. Hydrodynamic flow patterns, shock waves, and blast waves are examples of collective phenomena. On the other hand, coherence is used to refer to processes such as pionic instabilities that require a special phase relationships in many body wavefunctions. As we shall see, at the present only hints of collective phenomena have been seen. Signatures of coherent phenomena will be sought in subtle future experiments discussed later.

### 1) Single Proton Inclusive Cross Sections

The earliest hints of compression effects came from emulsion studies of Schopper et al.[8] However, statistical uncertainties in the data raised many questions as to the significance of those findings. Early LBL experiments found no evidence of Mach cones. However, little attempt was made to isolate central collisions in those experiments, and only impact parameter averaged data were studied.

In the most recent experiment by Gutbrod, Poskanzer, Stock, et al.[9] a first attempt to select central collisions was made by triggering on high associated multiplicities, M. The remarkable observation made for asymmetric systems, Ne+(Au,U) → p+X, at 400 MeV/nucleon was that the proton spectrum, $d\sigma/dEd\Omega$, peaked broadly around $\theta_{lab} \approx 30°$ for $E_{lab} \gtrsim 40$ MeV for events selected on high associated multiplicities. In Fig. 2, the preliminary data on Ne+Au are shown.[9] In Fig. 2a the proton spectra with low associated multiplicities are shown. Although the statistical fluctuations of the 20°, 30° data above 40 MeV are large, for a fixed E we see that

$$d\sigma(20°) \gtrsim d\sigma(30°) \gg d\sigma(90°) \gg d\sigma(150°) \quad , \qquad (5)$$

over the whole range $10 < E < 100$ MeV. Above 100 MeV, $d\sigma(20°)$ was found to be clearly greater than $d\sigma(30°)$.

In contrast, events with high associated multiplicity in Fig. 2b show an inverted order

$$d\sigma(30°) \gtrsim d\sigma(90°) \gtrsim d\sigma(20°) \gg d\sigma(150°), \qquad (6)$$

especially below 60 MeV. Note that the 90° and 150° spectra in both Figs. 2a,b are very similar above 40 MeV. However, the forward yield at 20°, 30° is greatly suppressed in Fig. 2b when high multiplicities are demanded as compared to Fig. 2a. Similar results were seen in Ne+U, but in Ne+Al (near symmetric system) this sideways peaking was not observed.

This effect is very suggestive of a hydrodynamic side splash as calculated by Nix et al. for $b < R_T$. This side splash, seen in Fig. 2c, is due simply to the fact that there are fewer mean free paths sideways than in the forward direction. Similar effects were also calculated by Stöcker et al. recently.[10]

An alternate source of broad 30° peaking could be shock waves formed in central $b \ll R_T$ collisions. To distinguish between side splash and shock phenomena, the $\phi$ distribution of the associated multiplicity must also be studied. Such studies are in progress.

While such structures in the proton spectra are indeed suggestive of collective hydrodynamic phenomena, they are of course not conclusive. It will be important to demonstrate via cascade calculations, for example, that such structures are not due to the non-equilibrium, few scattering component. Further theoretical studies with hydrodynamic codes will also be necessary to determine whether such hydrodynamic phenomena are sensitive to the equation of state of nuclear matter.

2) Single Pion Inclusive Cross Sections

The next interesting hint of collective phenomena was seen by Wolf et al.[11] in Ar+Ca $\rightarrow \pi^+ + X$ at 1 GeV/nucleon. The unusual nature of pion emission in this reaction is seen by comparing Fig. 3a to 3b. In Fig. 3b the characteristic emission pattern of $\pi^+$ from pp collisions at 730 MeV clearly shows the $\Delta_{33}(1232)$ decay pattern for a $\Delta$ at rest in the c.m. The yield is strongly suppressed in the mid rapidity, $p_\perp/m_\pi < 0.5$ region. In contrast, the yield in Ar+Ca has a maximum in that mid rapidity region at ($y = y_{p/2}$, $p_\perp/m \approx 0.4$). This qualitative difference is absent however at lower beam energies (400 MeV/nucleon). Furthermore, similar enhancement of mid rapidity, finite $p_\perp$ yield was seen by Nakai et al. (to be published) in Ne+NaF $\rightarrow \pi^+$ at 800 MeV/nucleon.

The cross section pattern in Fig. 3a is quite unexpected. In the fireball and streak models, the pion yield is isotropic in the c.m. with an exponentially decaying c.m. energy spectrum.[5] Cascade calculations also

fail to reproduce these features.[11]

A possible mechanism for this $\theta_{c.m.} = 90°$, $p_\perp/m \approx 0.4$ peak could be final state interactions due to nuclear shadowing and Coulomb repulsion. However, the pattern does not appear to change significantly when large associated multiplicities and hence more central collisions are isolated.[11] This insensitivity to associated multiplicities is not consistent with the assumption that final state interactions are responsible for that pattern.

This pattern therefore hints strongly of hydrodynamical flow effects that lead to preferential 90° ejection of pions in A on A collisions as predicted in hydrodynamic models.[12]

Another significant feature of the pion spectra that supports hydrodynamic flow effects is the observation that the at high c.m. energies and $\theta_{c.m.} = 90°$, $d^2\sigma(\pi) \propto e^{-E_\pi/T_\pi}$, where the apparent pion temperature $T_\pi$ is <u>less</u> than the apparent temperature of protons, $T_p$. This has been observed by Nagamiya et al.[3], and interpreted by P. Siemens[13] as evidence for a blast wave in nuclear collisions. See further discussion of this effect elsewhere in these proceedings and in Ref. (13).

3) Negative Pion Multiplicities and Distributions

One of the possible signatures[10] of collective phenomena involving density isomers is a discontinuity of the average number of $\pi^-$, $\langle n_\pi \rangle$, versus beam energy $E_p$. The first preliminary data on this excitation function are now available from Sandoval et al.[14] and shown in Fig. 4a. The $\langle n_\pi \rangle$ appears to grow linearly between 1 and 2 GeV/nucleon. The errors do not include possibly substantial systematic errors, and hence the deviation at 1.4 GeV/nucleon from a straight line is not significant. Nevertheless, we should keep an eye out for irregularities as the data become more precise. Also shown in Fig. 4a are calculations of $\langle n_\pi \rangle$ based on the thermal model in Ref. (15). At present $\langle n_\pi \rangle$ vs $E_p$ seems to be accounted for without invoking collective effects.

Next we discuss the negative pion multiplicity distribution $P(n_\pi)$. As shown in Ref. (15), $P(n_\pi)$ is expected to be a Poisson for a fixed impact parameter in a very large class of dynamical models. Only if there existed some unusual multi $\pi^-$ absorption or production mechanism would deviations from Poisson behavior be expected. Recent streamer chamber data of Sandoval et al.[14] test for the first time the Poisson form of $P(n_\pi)$ in central collisions. The data are shown in Fig. 4b along with the thermal model calculation based on Ref. (15). The maximum impact parameter corresponding to the central trigger is determined to be b = 3 fm by fitting $\langle n_\pi \rangle$ for that reaction. As seen in Fig. 4b, once $\langle n_\pi \rangle$ is fitted the entire shape of $P(n_\pi)$ is well reproduced by the Poisson form integrated from b = 0 to 3 fm. Thus at present, there is no evidence of multi $\pi^-$ cluster mechanisms.

While the pion momentum distribution show unexpected patterns in Fig. 3, the $\pi^-$ multiplicity data seem to be consistent with our naive expectations.

4) $\pi^-\pi^-$ Correlation Function $R(\tilde{k}_1,\tilde{k}_2)$

To search for coherent phenomena such as pion field instabilities,[16] we must turn to more subtle observables such as correlation functions. It is well known that identical boson or fermion correlation functions can be used to determine the space-time geometry of the interaction region. This is due to the famous Hanbury-Brown and Twiss effect. Correlation studies can therefore give a handle on the geometry of nuclear collisions. The first data[17] on the $\pi^-\pi^-$ correlations are now available and shown in Fig. 5a. The correlation function $R(k_1k_2)$ is the ratio of the coincidence rate of $2\pi^-$ with momenta $\tilde{k}_1$ and $\tilde{k}_2$ to the random counting rate of pion pairs with that momento.

In the absence of coherence in the pion field, $R(\tilde{k}_1-\tilde{k}_2) = 1 + |\rho(\tilde{k}_1-\tilde{k}_2)|^2$, where $\rho(q)$ is the Fourier transform of the pion production region. However, if the pion field has a degree of coherence, $D(\tilde{k})$, for mode $\tilde{k}$, then as shown in Ref. (18)

$$R(\tilde{k},\tilde{k}) = 2 - D^2(\tilde{k}) \qquad (5)$$

Thus, R can be used to measure the degree of coherence of the pion field.

There is an important source of potential error however, due to final state interactions. To unfold the distortions[18] of $R(k_1,k_2)$ requires detailed measurement of R as a function of both $\tilde{k} = \tilde{k}_1 + \tilde{k}_2$ and $\tilde{q} = \tilde{k}_1 - \tilde{k}_2$. The data[17] in Fig. 5a are averaged over $\tilde{k}$ and impact parameters and therefore final state distortions cannot at present be unfolded from the data. Nevertheless, the interaction sizes deduced from them are qualitatively reasonable. Determination of $D(\tilde{k})$ will be possible only after more refined measurements of R, which are in progress (K. Crowe, et al.), are completed.

We show in Fig. 5b the expected form of the correlation function for various degrees of coherence, D(k), and a Gaussian interaction region of radius $R_0$ as calculated in Ref. (18).

5) pp Large Angle Correlations

While experiments on small angle pp correlations will supplement the $\pi^-\pi^-$ correlation experiments in determining the space-time geometry of nuclear collisions, large angle pp correlations offer an exciting new handle in the search for coherent phenomena such as critical scattering discussed in Ref. (16).

Recently, Nagamiya et al.[3] have been able to isolate the quasi-elastic (direct) component via correlation measurements. In Fig. 6a, the ratio of in plane coincidence rate, $R(\theta, \Delta\phi = 180°)$, to the out of plane coincidence rate $R(\theta,\Delta\phi = 90°)$ for two protons from $C+C \rightarrow p+p + X$ at 800 MeV/nucleon is plotted. The trigger proton is detected at $\theta_{c.m.} \approx 90°$, $\phi = 0°$ and $E_{c.m.} \approx 200$ MeV. The second proton is measured in a spectrometer at

at $\phi = \pm 90°$ or $180°$ to get this ratio. A clear quasi-elastic peak is seen for C+C in Fig. 6a at $\theta_{lab} \approx 40° \Rightarrow \theta_{c.m.} \approx 90°$, $\phi = 180°$. (The evidence for nuclear shadowing is seen in C+Pb for which the ratio $\approx 0.9 < 1.0$.) This measurement can be used to deduce the fraction $f_{el}(\theta_{c.m.})$ of quasi-elastic scattering at $\theta_{c.m.} = 90°$.

The new proposal by Tanihata et al. is to measure $f_{el}(\theta_{c.m.})$ at other $\theta_{c.m.}$ via such correlations. Comparing the shape of $f_{el}(\theta_{c.m.})$ to the elementary, $d\sigma(p+p \rightarrow p+p)/d\Omega_{c.m.}$, angular distribution, the signatures of critical scattering[16] phenomena would be an enhanced yield at finite angles. The feature of critical scattering phenomena associated with pionic instabilities that is most easily tested and least model dependent is that the enhancement of $f_{el}(\theta_{c.m.})$ would occur for $\theta_{c.m.}$ corresponding to a momentum transfer $q \sim 1\text{-}2\ m_\pi$ as illustrated in Fig. 6b.

Further cascade code studies will be necessary to insure proper background subtraction, but potentially this experiment will give a powerful tool in the search for coherent processes.

## IV. SUMMARY (See Table II)

We may be at last getting the first hints of collective phenomena in relativistic nuclear collisions: 1) side peaking of proton yield[9] at $\theta_{lab} \approx 30°$ associated with high multiplicities, 2) $\theta_{c.m.} = 90°$, $p_\perp/m_\pi \approx 0.4$ enhancement[11] of $\pi^+$ yield, and 3) $T_\pi < T_p$ at $\theta_{c.m.} = 90°$, high $p_\perp$.[13] Furthermore the search for signatures of coherent phenomena are now well underway via $\pi^-\pi^-$ and pp correlations. We have reached an exciting period with relativistic nuclear collisions. The physics is more fun than ever.

Acknowledgments: This work was supported by the Nuclear Physics Division of the U. S. Department of Energy under contract No. W-7405-eng-48. I am most grateful to H. Gutbrod, R. Stock, A. Sandoval, S. Nagamiya, K. Wolf, W. Benenson, I. Tanihata, L. Schroeder for making their preliminary data and viewpoints available. Discussions with P. Siemens, J. Randrup, and W. D. Myers were also valuable in preparation of this brief review.

## REFERENCES

1. For reviews and references on the first generation of nuclear collision studies see, M. Gyulassy, LBL-6594 preprint (Oct. 1977); R. Nix, Los Alamos preprint LA-UR-77-2952 (Dec. 1977); A. Goldhaber, H. Heckman, Ann. Rev. Nucl. Part. Sci. 28, 161 (1978); Proceedings of Symposium on Relativistic Heavy Ion Research, GSI-p-5-78, July 1978, GSI Darmstadt, Vols, I, II; The 4th High Energy Heavy Ion Summer Study, LBL-7766, UC-34C, Conf-780766, July 1978.

2. J. Knoll, J. Randrup, Nordita preprint 78/48, Nov. 1978.

3. S. Nagamiya, et. al., Phys. Lett. 81B, 147 (1979).

4. W. Benenson, et. al., to be published.

5. Gosset, J., et al, Phys. Rev. C 18, 844 (1978).

6. M. C. Lemaire, et. al., LBL-8978 preprint, April 1979.

7. J. Vary, private communication.

8. H. G. Baumgart, et. al., Z. Physik A 273, 359 (1975).

9. See p. 52-63 of LBL-7766 Ref. (1). Fig. 2 was prepared by H. Gutbrod using latest unpublished data.

10. See talk of W. Greiner elsewhere in proceedings.

11. K. L. Wolf, et. al., Phys. Rev. Lett. 42, 1448 (1979).

12. W. Scheid, et. al., Phys. Rev. Lett. 32, 741 (1974).

13. P. J. Siemens, J. O. Rasmussen, Phys. Rev. Lett. 42, 880 (1979).

14. A. Sandoval et. al., to be published.

15. M. Gyulassy, S. K. Kauffmann, Phys. Rev. Lett. 40, 298 (1978).

16. M. Gyulassy, W. Greiner, Ann. Phys. 109, 485 (1977).

17. S. Y. Fung, et. al., Phys. Rev. Lett. 41, 1592 (1978).

18. M. Gyulassy, S. K. Kauffmann, Lance W. Wilson, LBL-8759 preprint, April 1979, and refs. therein.

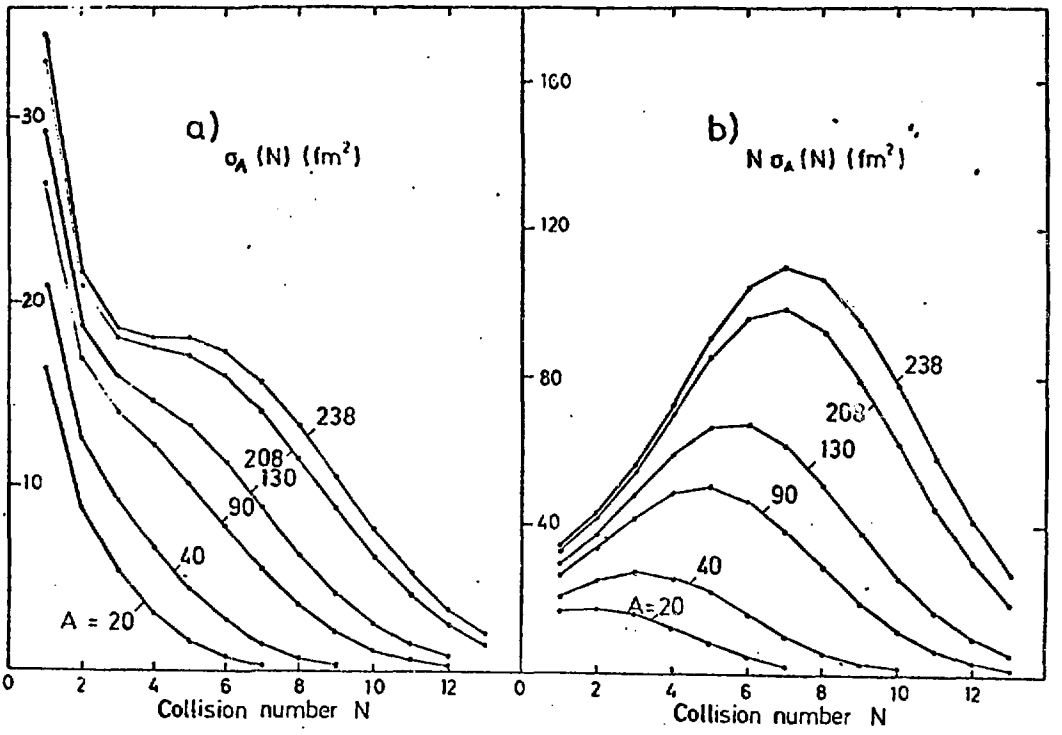


Fig.1 a) Distribution[2] of number of binary collisions of one nucleon on nucleus A. b) same for A+A collisions at b=0.

Table I. Percent of nucleons in $A_p$=$A_T$ central collisions (b=0) that scatter only once (direct), more then four times (thermal) and intermediate.

| System | Direct (N=1) | Intermediate | Thermal (N>4) |
|---|---|---|---|
| Ne + Ne | 21 | 42 | 37 |
| Ar + Ar | 13 | 33 | 54 |
| Xe + Xe | 6 | 17 | 77 |
| U + U | 4 | 11 | 85 |

Table II: Current Observables Used in the Search for High Density Phenomena in Relativistic Nuclear Collisions

| | Observable | System | Impact Range | Phenomena | Signature | Experimental Status |
|---|---|---|---|---|---|---|
| 1. | $d\sigma(p)$ | $A_p \ll A_T$ | $b<R_T$ | hydrodynamic side splash | peak at $\Theta_{Lab}>0$ | + |
| 2. | $d\sigma(p)$ | $A_p \ll A_T$ | $b \ll R_T$ | shock wave | peak at $\Theta_{Lab}>0$ | ? |
| 3. | $d\sigma(\pi)$ | $A_p=A_T$ | $b<R_T$ | blast wave | $T_\pi<T_p$ | + |
| 4. | $\langle n_\pi^- \rangle$ | $A_p=A_T$ | $b \ll R_T$ | density isomerism | discontinuity $\langle n_\pi \rangle$ vs $E_{Beam}$ | ? |
| 5. | $p(n_\pi^-)$ | $A_p=A_T$ | $b \ll R_T$ | multipion cluster mechanism | non-Poisson tail | - |
| 6. | $d\sigma(\pi^-\pi^-)$ | $A_p=A_T$ | $b \ll R_T$ | pion field coherence | $R(\tilde{k},\tilde{k})<2$ | in progress |
| 7. | $d\sigma(pp)$ | $A_p=A_T$ | $b \ll R_T$ | pionic instabilities | critical scattering | in progress |

Note: $d\sigma(F_1)$, $d\sigma(F_1F_2)$ denote single and double inclusive cross sections for fragments $F_1F_2$, $\langle n_\pi^- \rangle$ is the average negative pion multiplicity, $p(n_\pi^-)$ is the negative pion multiplicity distribution. The impact range $b<R_T$ corresponds to high associated multiplicites with azymuthal asymmetry, while $b \ll R_T$ corresponds to central collisions with azymuthal symmetry. Status + indicates positive observation of signature although implications may still be under debate; ? indicates conflicting or uncertain observations; - indicates no evidence observed.

Fig.2 Preliminary data[9] on Ne+Au → p+X at 400 Mev/nucleon for a class of events with a) low associated multiplicities ($M \leq 6$) and b) high associated multiplicities ($M > 15$). Plotted are $d^2\sigma/dEd\Omega$ (mb/sr.Mev) for various $\theta_{lab}$ vs. $E_{lab}$.

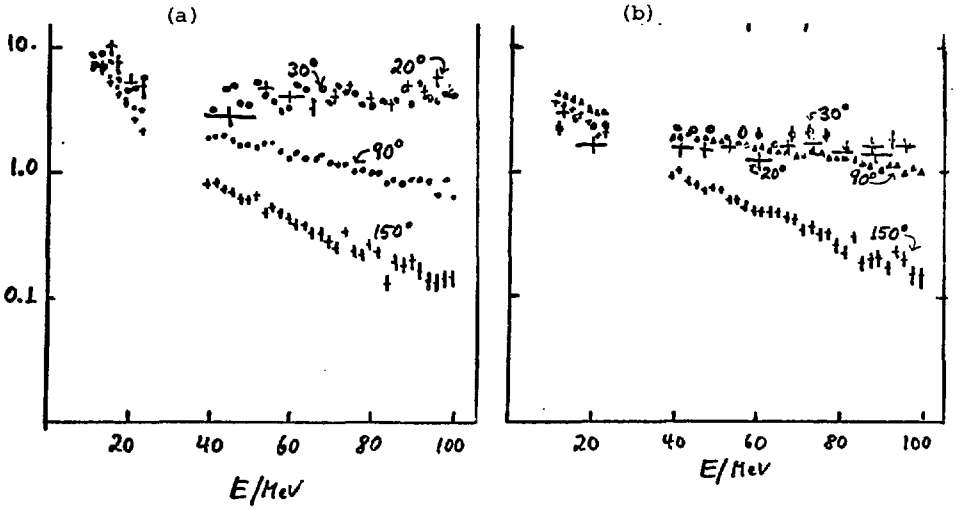


(c) Hydrodynamic results of Nix et.al.[1] for Ne+U → p+X at 250 Mev/nucleon for b=5.4fm illustrating side splash effect.

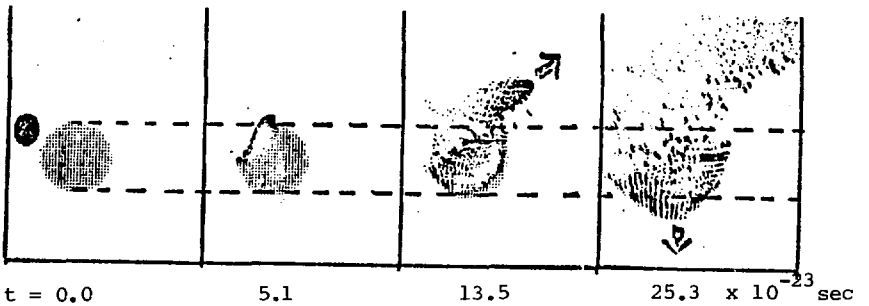

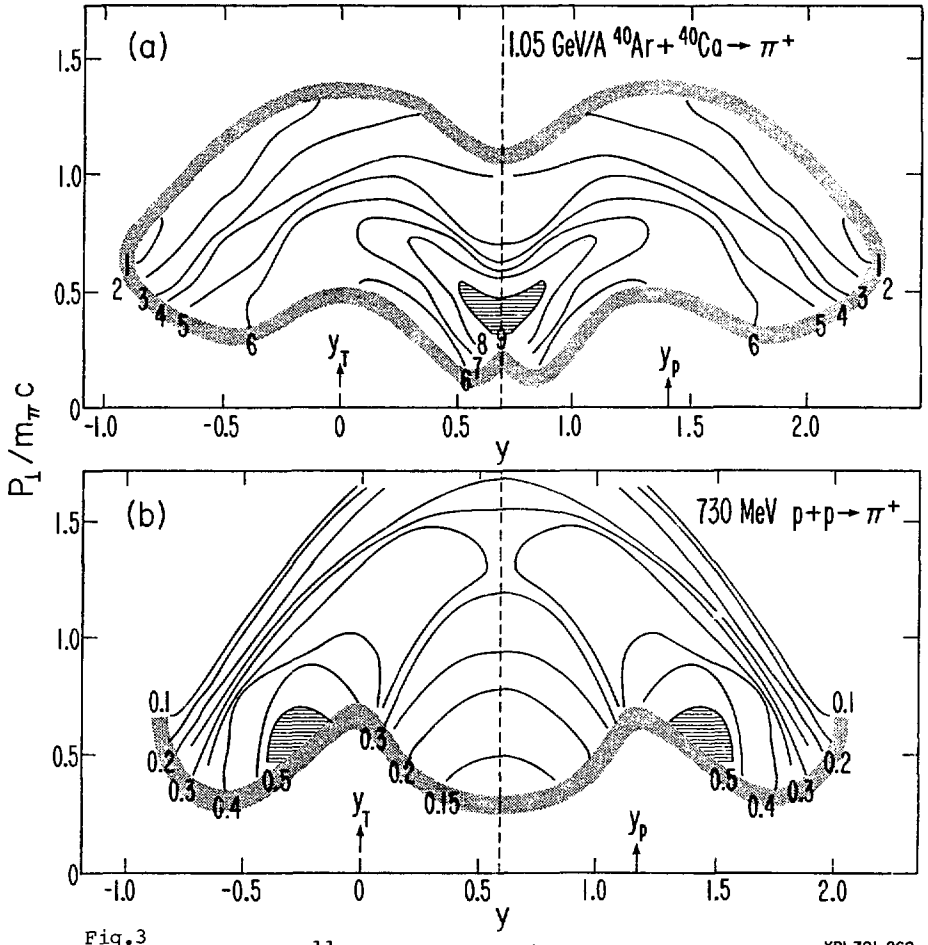


Fig.3 XBL791-260

Contour plot[11] of invariant $\pi^+$ inclusive cross section for (a) nucleus-nucleus collision and (b) proton-proton collision at about same energy per nucleon. Dashed line shows c.m. rapidity; horizontal shaded areas correspond to maximum yield regions.

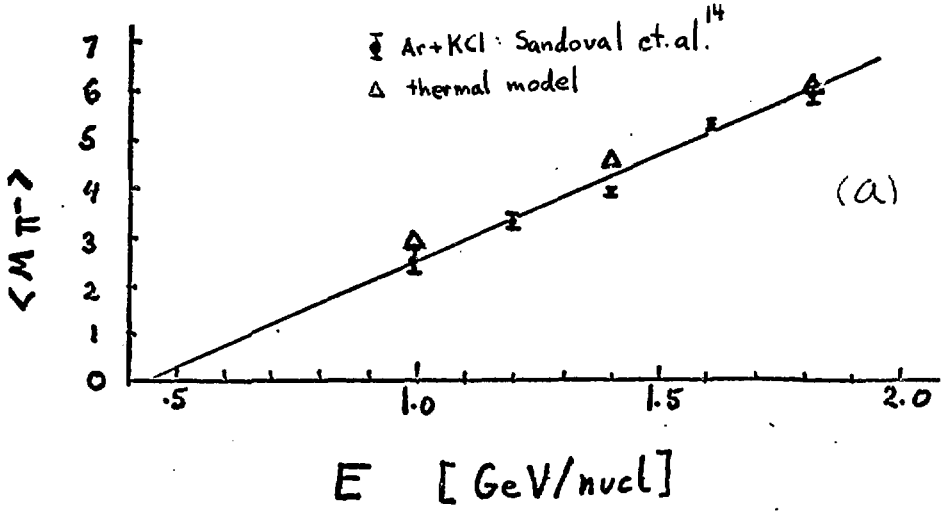


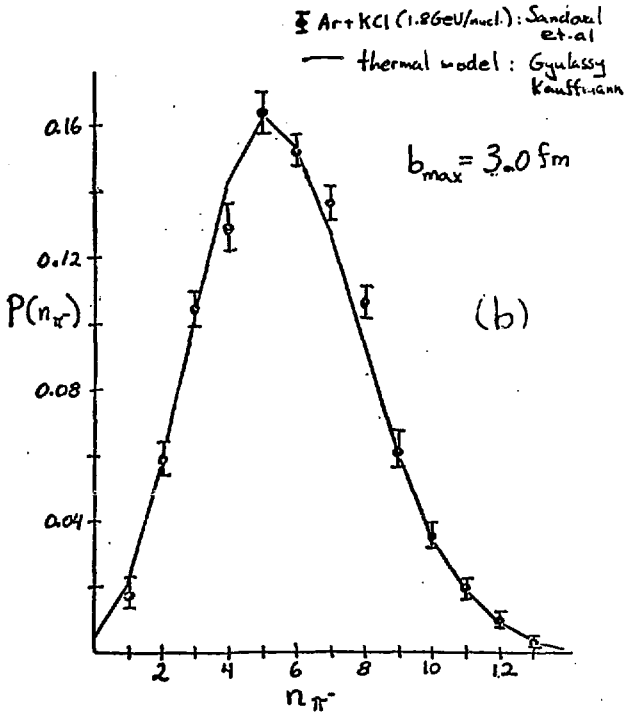


FIG. 4

Preliminary data by Sandoval et. al.[14] on a) Average negative pion multiplicity $\langle m_{\pi^-} \rangle$ versus beam energy and b) multiplicity distribution in central trigger mode for Ar+KCl. Thermal model[15] results are also indicated.

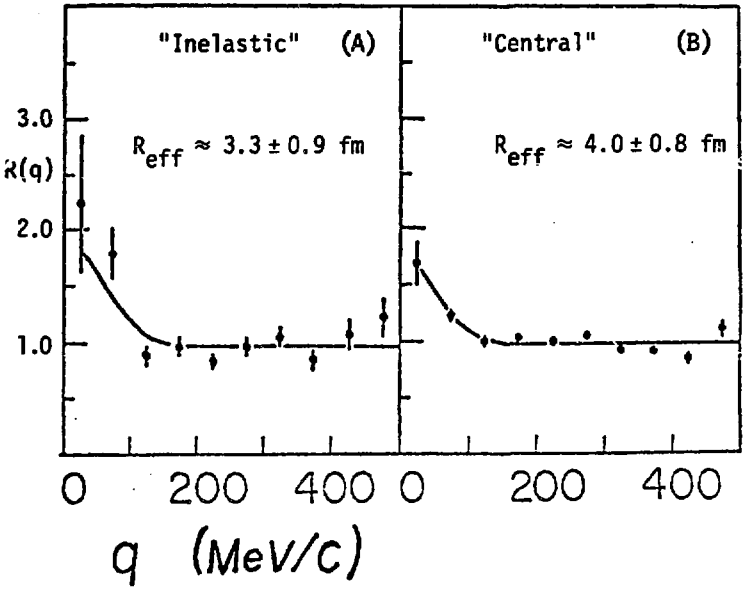


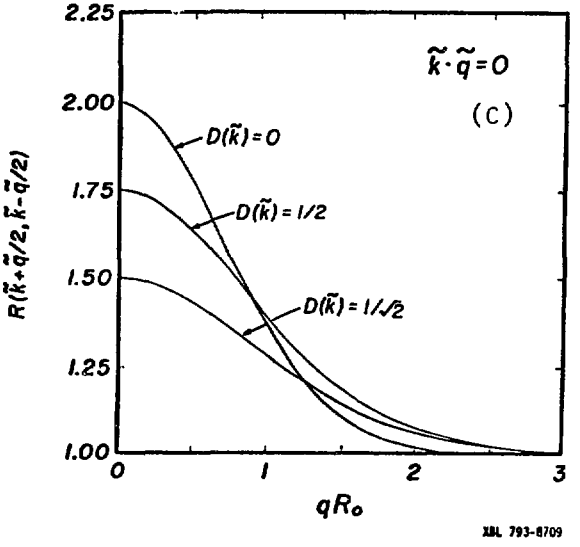


Fig. 5

(A, B) First data[17] on $\pi^-\pi^-$ correlations for $Ar+Pb_3O_4$ at 1.8 GeV/nucleon. Source radius deduced is indicated for two trigger modes. (C) Theoretical correlation [18] function for finite degree of coherence D(k) and gaussian source distribution of radius $R_o$.

(A)

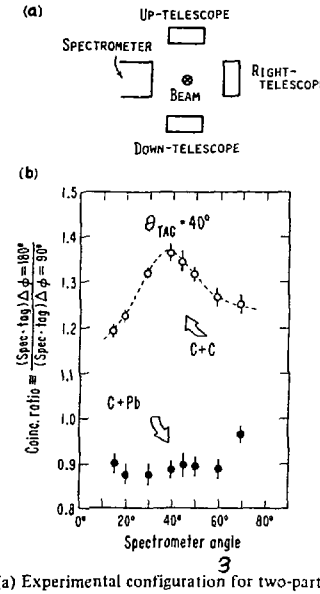


Fig.6 (A) (a) Experimental configuration for two-particle correlation measurements. (b) Degree of coplanarity $C$ for all charged particle emission plotted as a function of the spectrometer angle $\theta_{SP}$. Absolute scale of vertical axis is reliable within an error of ± 0.1.
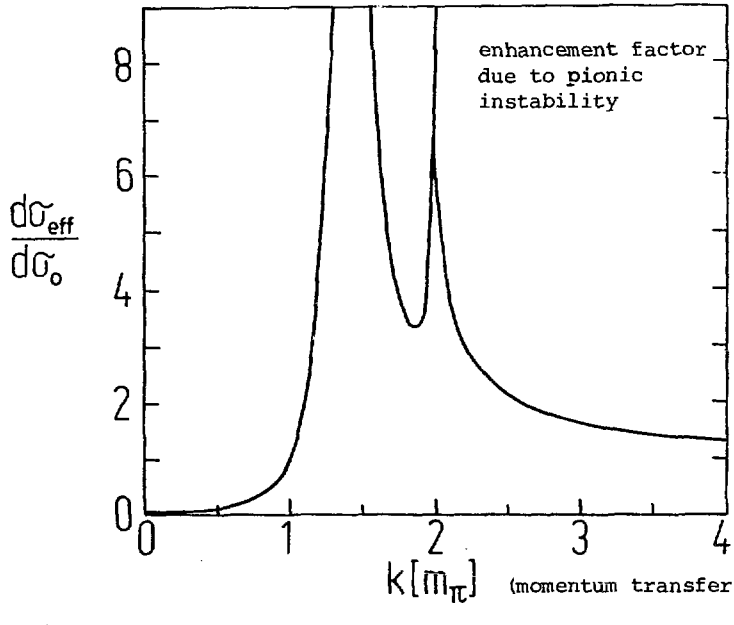
(B) Calculated[16] example of critical scattering